

Nonthermal neutrino-like hot dark matter in light of the S_8 tension

Subinoy Das^{1,*}, Anshuman Maharana^{2,†}, Vivian Poulin^{3,‡} and Ravi Kumar Sharma^{1,§}

¹Indian Institute of Astrophysics, Bengaluru, Karnataka 560034, India

²Harish-Chandra Research Institute, A CI of Homi Bhabha National Institute, Allahabad 211019, India

³Laboratoire Univers et Particules de Montpellier (LUPM), CNRS
and Université de Montpellier (UMR-5299), Place Eugène Bataillon,
F-34095 Montpellier Cedex 05, France



(Received 22 April 2021; accepted 9 March 2022; published 4 May 2022)

The Λ CDM prediction of $S_8 \equiv \sigma_8(\Omega_m/0.3)^{0.5}$ —where σ_8 is the root mean square of matter fluctuations on an $8 h^{-1}$ Mpc scale—once calibrated on Planck cosmic microwave background data is $2 - 3\sigma$ lower than its direct estimate by a number of weak lensing surveys. In this paper, we explore the possibility that the “ S_8 tension” is due to a fractional contribution of nonthermal hot dark matter (HDM) to the energy density of the Universe leading to a power suppression at small scales in the matter power spectrum. Any HDM model can be characterized by its effective mass $m_{\text{sp}}^{\text{eff}}$ and its contribution to the relativistic degrees of freedom at cosmic microwave background decoupling ΔN_{eff} . Taking the specific example of a sterile particle produced from the decay of the inflaton during an early matter-dominated era, we find that the tension can be reduced below 2σ from Planck data only, but it does not favor a nonzero $\{m_{\text{sp}}^{\text{eff}}, \Delta N_{\text{eff}}\}$. In combination with a measurement of S_8 from KiDS1000 + BOSS + 2dfLenS, the S_8 tension would hint at the existence of a particle of mass $m_{\text{sp}}^{\text{eff}} \simeq 0.67_{-0.48}^{+0.26}$ eV with a contribution to $\Delta N_{\text{eff}} \simeq 0.06 \pm 0.05$. However, Pantheon and BOSS BAO/ $f\sigma_8$ data restricts the particle mass to $m_{\text{sp}}^{\text{eff}} \simeq 0.48_{-0.36}^{+0.17}$ and contribution to $\Delta N_{\text{eff}} \simeq 0.046_{-0.031}^{+0.004}$. We discuss implications of our results for other canonical nonthermal HDM models—the Dodelson-Widrow model and a hidden sector model of a thermal sterile particle with a different temperature. We report competitive results on such hidden sector temperature that might have interesting implications for particle physics model building, in particular connecting the S_8 tension to the longstanding short baseline oscillation anomaly.

DOI: [10.1103/PhysRevD.105.103503](https://doi.org/10.1103/PhysRevD.105.103503)

I. INTRODUCTION

The Λ cold dark matter (Λ CDM) model of cosmology is compelling at describing a wide variety of observations up to a high degree of accuracy despite the nature of its dominant components—CDM and dark energy (DE)—still being unknown. Nevertheless, in recent years, a number of intriguing discrepancies have emerged between the values of some cosmological parameter predicted within Λ CDM—once the model is calibrated onto Planck cosmic microwave background (CMB) data, baryon acoustic oscillation (BAO), and luminosity distance to supernovae of type Ia (SNIa)—and their direct measurements.

At the heart of this study is the longstanding tension affecting the determination of the amplitude of matter fluctuations, typically parametrized as $S_8 \equiv \sigma_8(\Omega_m/0.3)^{0.5}$, where σ_8 is the root mean square of matter

fluctuations on an $8 h^{-1}$ Mpc scale, and Ω_m is the total matter abundance. The latest prediction from Planck CMB data within the Λ CDM framework is $S_8 = 0.832 \pm 0.013$ [1]. Originally, observations of galaxies through weak lensing by the CFHTLenS collaboration have indicated that the Λ CDM model predicts a S_8 value that is larger than the direct measurement at the 2σ level [2,3]. This tension has since then been further established within the KiDS/Viking data [4,5], but is milder within the DES data [6]. However, a reanalysis of the DES data, combined with KiDS/Viking, led to a determination of S_8 that is discrepant with *Planck* at the 3σ level, $S_8 = 0.755_{-0.021}^{+0.019}$ [5]. Recently, the combination of KiDS/Viking and SDSS data has established $S_8 = 0.766_{-0.014}^{+0.02}$ [7]. Moreover, it is now understood that the tension is driven by a lower matter clustering amplitude σ_8 . This is mainly due to the fact that Ω_M is strongly constrained—even in extension from Λ CDM—from the observations of uncalibrated luminosity distance to supernovae and baryonic acoustic oscillations. This is particularly interesting for model building: resolving the S_8 tension requires us to decrease the amplitude of

* subinoy@iiap.res.in

† anshumanmaharana@hri.res.in

‡ vivian.poulin@umontpellier.fr

§ ravi.sharma@iiap.res.in

matter fluctuations on scales $k \sim 0.1\text{--}1 h/\text{Mpc}$, which can be easily achieved in a variety of models often related to new DM properties [8–20], or new neutrino properties [21,22].

In this paper, we explore the possibility that the “ S_8 tension” is due to the existence of a nonthermal hot dark matter (HDM) consisting of light sterile neutrinos or hidden sector particles contributing to a fraction of the dark matter (DM) density in the Universe, and leading to a power suppression at small scales in the matter power spectrum. It is well known that just adding a thermal neutrino-like radiation ΔN_{eff} , together with a nonzero neutrino mass m_ν , does not resolve the S_8 problem [1,21]. Here, we explore the consequences of a nonthermal momentum distribution for the hot component (or a temperature different from our visible sector), for the S_8 tension. In practice, we consider the momentum distribution associated with sterile particles produced from decays during an early matter domination to radiation domination transition of the Universe. We refer to the model as $\nu_{\text{NT}}\Lambda\text{CDM}$. From the point of view of theoretical models, it is natural for the early Universe to enter an epoch of early matter-dominated era (EMDE) [23–25]. This EMDE epoch transitions to the radiation-dominated era through the decay of the inflaton or cold moduli, which dominate the energy density of the Universe at early times, or EMDE can also appear from hidden sector physics [26,27]. In string and theories of supergravity, this occurs due to moduli vacuum misalignment [28–30]. For detailed arguments on the generality of this and computations in explicit settings see, e.g., Refs. [31–33].

It was shown that the decay products obtain a characteristic momentum distribution [34–37] that is associated with decays taking place in a matter-dominated Universe evolving to radiation domination. The momentum distribution function is essentially fixed by the kinematics. Of course, this happens only under certain conditions, these are as follows: the particles arise from a $1 \rightarrow 2$ decay of the unstable particle (whose quanta dominate the energy density of the Universe) and have a mass much smaller than the mass of the decaying particle. Furthermore, the particles will be taken to be inert, so that they free stream after production. Thermalization of the decay products leads to the loss of all information about the kinematics of the decay process. But in a setting with a large number of hidden sectors, one can expect that some of the species produced during the decay do not thermalize due to very weak interactions. Our scenario belongs to a category where a moduli or inflaton field decays to nonthermal sterile particles. There might be other particles such as a feebly interacting massive particle that can also produce nonthermal or partially thermal neutrino-like particles [38]. The presence of nonthermal dark radiation can affect the CMB [39] as well as large-scale structures in specific ways and can be probed by precision cosmological data. The study of the implications of sterile particles with this momentum distribution for precision cosmology was

recently initiated¹ in Ref. [37]. Given that the effect of massive sterile particles on the CMB and matter power spectra is well known (e.g., [41–43] for reviews), it was anticipated there one might get a substantial power suppression in the matter power spectrum due to the momentum distribution of the nonthermal decay products. This power suppression has implications for the S_8 tension.

In this article, we perform a comprehensive Monte Carlo Markov chain (MCMC) analysis against up-to-date data from *Planck*, BOSS (BAO and redshift space distortions $f\sigma_8$), and Pantheon data, with and without the inclusion of a prior on the value of S_8 as measured with the KiDS/Viking + BOSS + 2dFLens data.² We find that the $\nu_{\text{NT}}\Lambda\text{CDM}$ model can indeed alleviate the tension between *Planck* and S_8 measurements, but the success of the resolution is slightly degraded once BOSS and Pantheon data are included in the analysis. To better understand the features of the model leading to a resolution of the tension, we compare the nonthermal sterile neutrino model to the standard massive neutrino model with extra relativistic degrees of freedom. We find that, for a similar effect on the CMB power spectrum, the $\nu_{\text{NT}}\Lambda\text{CDM}$ leads to a much stronger suppression in the matter power spectrum at late times, and therefore to a more significant decrease in σ_8 . The impact of the $\nu_{\text{NT}}\Lambda\text{CDM}$ is barely visible on the BAO scale and luminosity distance, but it does affect $f\sigma_8$ predictions. The model is therefore further constrained by BOSS redshift space distortions data. Future measurements of the matter power spectrum and $f\sigma_8$ at late times will further test this scenario [47].

Although the MCMC analysis is carried out for sterile particles with the above-described momentum distributions, it has implications for a wide class of models. As is well known (see, e.g., [41,48]), the cosmological implications of a hot and sterile component is captured effectively by just two parameters: (i) the contribution of the component to the present-day energy density, usually reported in terms of the effective mass parameter m_{eff} ; (ii) the contribution of the component to the energy density at the time of the CMB decoupling, usually reported in terms of ΔN_{eff} .³ These parameters are determined by the first two moments of the momentum distribution and the mass of the sterile particle. Two models with equal values of m_{eff} and ΔN_{eff} will have the same phenomenological effects even if the form of the momentum distribution is different. We use these properties to translate the results of

¹For earlier in work on inert particles from decays see, e.g., [34–36,40].

²For analysis in similar spirit (although without inclusion of the S_8) prior motivated by short base line neutrino experiments see, e.g., [44,45]. Of course, here the momentum distribution of the sterile particles is assumed to be as motivated by neutrino physics, i.e., thermal or the Dodelson-Widrow distribution [46].

³In the models we will discuss, this is same as ΔN_{eff} at the time of neutrino decoupling.

the analysis for our model parameters to results on the effective parameters. Our results, therefore, have direct implications for other well-motivated momentum distributions such as a thermal distribution with a different temperature from that of the Standard Model [49–52], the Dodelson-Widrow distribution [46] or distributions similar to the Dodelson-Widrow discussed in Refs. [53,54].

Our paper is structured as follows: in Sec. II, we present our model and the mapping onto generic phenomenological parameters; in Sec. III, we perform an MCMC analysis against a suite of up-to-date cosmological data and discuss the extent to which the $\nu_{\text{NT}}\Lambda\text{CDM}$ can resolve the S_8 tension; in Sec. IV, we draw implications of our results for other HDM models; finally, we conclude in Sec. V.

II. NONTHERMAL HOT DARK MATTER

A. The model

The physics of a constituent species of dark matter depends on its mass, interactions, and also on its momentum distribution function. For species that thermalize, the process of thermalization brings the momentum distribution to the Fermi-Dirac or Bose-Einstein form. On the other hand, for nonthermal constituents the momentum distribution is determined by their production mechanism. Thus, it is important to isolate natural production mechanisms for species that can constitute the dark matter, the associated momentum distribution, and their implications for cosmology.

In this section, we will review the basics of the production mechanism and the form of the momentum distribution that we will be considering. Our discussion will be brief, we refer the reader to Ref. [37] and the references therein for details. At early times, the energy density of the Universe will be taken to be dominated by cold particles of a species φ . We will denote the mass of the particles of φ by m_φ and their decay width to be τ . We will be focusing on the case when the φ is the inflaton, with inflation taking place at the GUT scale and decays of the inflaton taking place due to a nonrenormalizable interaction at the GUT scale. Thus, we take $m_\varphi \sim 10^{-6}M_{\text{pl}}$ and $\tau \sim 10^8/m_\varphi$. The branching ratio of the φ particles to the sterile particles will be taken to be B_{sp} , the sterile particles so produced will be taken not to thermalize. We will assume that the other decay products thermalize, as this sector would contain the Standard Model, we will refer to it as the Standard Model sector. All decay products will be taken to be relativistic at the time of production. As the φ particles decay, the Universe goes into a matter to radiation epoch, finally becoming fully radiation dominated.

During the matter to radiation-dominated epoch the evolution of the Universe is governed by the equations

$$\dot{\rho}_{\text{mat}} + 3H\rho_{\text{mat}} = -\frac{\rho_{\text{mat}}}{\tau}, \quad (1)$$

$$\dot{\rho}_{\text{rad}} + 4H\rho_{\text{rad}} = +\frac{\rho_{\text{mat}}}{\tau}, \quad (2)$$

and

$$H = \left(\frac{\dot{a}}{a}\right) = \sqrt{\frac{\rho_{\text{mat}} + \rho_{\text{rad}}}{3M_{\text{pl}}^2}}. \quad (3)$$

In the above, ρ_{mat} denotes the energy density in the matter and ρ_{rad} is the energy density in radiation. The energy density in radiation is the sum of the energy densities in the Standard Model sector and the sterile particles (since the sterile particles are highly relativistic at the time of production, they contribute to the energy density as radiation when decays take place). It is useful to introduce dimensionless variables.

$$\theta = \frac{t}{\tau}, \quad \hat{s}(\theta) = a(\tau\theta),$$

$$e_{\text{mat}}(\theta) = \frac{\tau^2 \rho_{\text{mat}}(\tau\theta)}{M_{\text{pl}}^2} \quad \text{and} \quad e_{\text{rad}}(\theta) = \frac{\tau^2 \rho_{\text{rad}}(\tau\theta)}{M_{\text{pl}}^2}. \quad (4)$$

Once almost all φ particles have decayed, one can take the Universe to be composed of a thermal bath (which contains the Standard Model sector) and the sterile particles governed by the standard cosmological evolution equations. In practice, we will start with a matter-dominated universe at an ‘‘initial time’’ ($t = \theta = 0$), evolve the universe using Eqs. (1), (2), and (3) up to a fiducial dimensionless time θ^* , which is large enough so that almost all the φ particles have decayed by that time (we will choose $\theta^* = 15$ in practice). We use the results of this procedure as initial conditions for the standard cosmological evolution. For the initial energy densities, we choose $e_{\text{mat}}(0) = \frac{4}{3}\alpha$ and $e_{\text{rad}}(0) = 0$, with $\alpha \gg 1$ (the factor of $4/3$ is included as it leads to some simplifications in the equations, for the numerical application we take $\alpha = 10^4$). This implies that initially the Universe is completely matter dominated, with the initial Hubble (H_{in}) satisfying $H_{\text{in}}\tau \gg 1$. This ensures that our results are independent of the choice of initial conditions.

The momentum distribution of the sterile particles can be computed from the fact that, as a result of the decays, the comoving number density of the sterile particles falls off as $N(t) = N(0)e^{-t/\tau}$ (with the branching ratio to the sterile particles being B_{sp}), and once produced the sterile particles free stream. We will be making use of publicly available package CLASS [43,55] to incorporate the effects of the sterile particles, which takes as input the momentum distribution of the sterile particles today. This was obtained in [37] to be

$$f(\vec{q}) = \frac{32}{\pi \hat{E}^3} \left(\frac{N(0)B_{\text{sp}}}{\hat{s}^3(\theta^*)} \right) \frac{e^{-\hat{s}^{-1}(y)}}{|\vec{q}|^3 \hat{H}(\hat{s}^{-1}(y))}, \quad (5)$$

where

$$y = \frac{|\vec{q}|}{4} \hat{s}(\theta^*), \quad (6)$$

and the argument of the function \vec{q} is constrained so that

$$\frac{4}{\hat{s}(\theta^*)} < |\vec{q}| < 4, \quad (7)$$

where $\hat{E} = m_\varphi/2$, $N(0)$ is the initial number density of the φ particles, $\hat{s}(\theta^*)$ is the value scale factor⁴ at the fiducial dimensionless time θ^* , \hat{s}^{-1} is the functional inverse of the scale factor function as a function of the dimensionless time, and $\hat{H} = \hat{s}'(\theta)/\hat{s}(\theta)$ is the dimensionless Hubble constant. The momentum \vec{q} in (5) is the momentum in units of the typical momentum magnitude of the sterile particles today ($T_{\text{ncdm},0}$). The typical momentum magnitude was found to be

$$T_{\text{ncdm},0} = 0.418 \left(\frac{m_\varphi^2 \tau}{M_{\text{pl}}} \right)^{1/2} \frac{T_{\text{cmb}}}{(1 - B_{\text{sp}})^{1/4}} \equiv \zeta T_{\text{cmb}} \quad (8)$$

in [37]. The distribution function in (5) is in units of $T_{\text{ncdm},0}^3$. Thus $f(\vec{q})d^3q$ gives the number density of particles with their dimensionless momentum in the interval $(q_i, q_i + dq_i)$ with the number density measured in units of $T_{\text{ncdm},0}^3$.

Note that although naïvely $f(\vec{q})$ seems to depend on $N(0)$, the full expression is independent of $N(0)$ as long as we take the universe to be completely matter-dominated at the initial time. It is interesting to compare the distribution to a thermal one, as shown in Fig. 1. We focus on the range $q \equiv |\vec{q}| \in [0.1, 1.2]$ because the distribution falls off beyond that range [37]. For the same value of ΔN_{eff} , the nonthermal distribution is peaked at higher values of the momentum but is much broader. The mean momentum of sterile particles is greater than that of the CMB by the factor ζ defined in (8). For our choice of parameters $\zeta \sim 5$. The sterile particles become nonrelativistic when their typical momentum becomes of the order of their mass, i.e., the temperature of the Standard Model plasma becomes of the order $m_{\text{sp}}/5$.

B. Mapping onto generic parameters

Our model has four microscopic parameters: m_φ , τ (the mass and lifetime of the decaying particle), B_{sp} (the branching ratio for decay to the sterile particle), and m_{sp} (the mass of the sterile particle) in addition to those of Λ CDM. Our choice of the first two parameters ($m_\varphi \sim 10^{-6} M_{\text{pl}}$ and $\tau \sim 10^8/m_\varphi$) is motivated by taking φ to be driving inflation at the GUT scale and decaying by

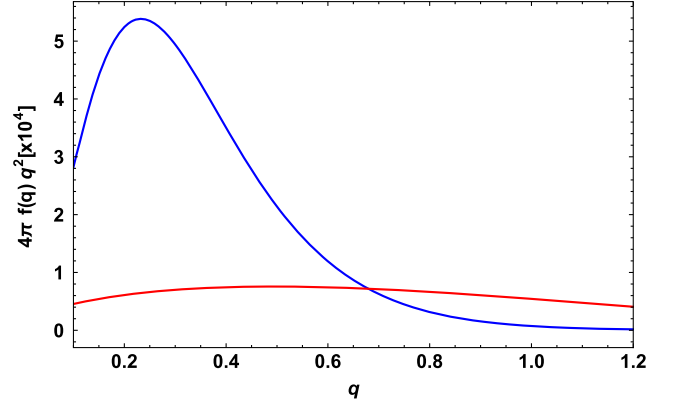


FIG. 1. Comparative plot with a thermal distribution. The nonthermal distribution is plotted in orange and is for value of the parameter $m_\varphi = 10^{-6} M_{\text{pl}}$, $\tau = 10^8/m_\varphi$. The thermal distribution is in blue. The momenta and the distribution functions for both plots are in units of $T_{\text{ncdm},0}$ as associated with the above values of m_φ and τ . ΔN_{eff} is taken to be 0.15 for both distributions. The x axis label $q \equiv |\vec{q}|$ as defined in the main text.

GUT scale interactions. On the other hand, the other parameters B_{sp} and m_{sp} will be traded for effective parameters more directly connected to observables. Indeed, the physical effects of new sterile particle/species on the cosmological background and perturbation evolution can be completely described by three parameters: ΔN_{eff} (the effective number of relativistic neutrinos at the time of neutrino decoupling), $w_{\text{sp}} \equiv \Omega_{\text{sp}} h^2$ (where Ω_{sp} is the fractional contribution of the particle to today's energy density and the reduced Hubble parameter, this is often characterized by the effective mass of the particle $m_{\text{sp}}^{\text{eff}} = w_{\text{sp}} 94.05 \text{ eV}$) and λ_{FS} (the free-streaming length associated with the species). The free-streaming length is determined once the first two quantities are known, hence effectively there are two parameters [41]. Physically, the two parameters of interest for reducing σ_8 are w_{sp} , which fixes the depth of the power suppression, and λ_{FS} , which fixes the scale above which modes are suppressed. Still, for their simpler connection with microphysics, here we take ΔN_{eff} and $m_{\text{sp}}^{\text{eff}}$ as two independent quantities, defined as

$$\Delta N_{\text{eff}} \equiv \frac{\rho_s^{\text{rel}}}{\rho_\nu} = \frac{1}{\pi^2} \left[\int dp p^3 \hat{f}(p) \right] / \left[\frac{7}{8} \frac{\pi^2}{15} T_\nu^{\text{id}4} \right], \quad (9)$$

with $T_\nu^{\text{id}} \equiv (4/11)^{1/3} T_\gamma$ and

$$\frac{m_{\text{sp}}^{\text{eff}}}{94.05 \text{ eV}} \equiv \omega_s \equiv \Omega_s h^2 = \frac{1}{\pi^2} \left[m_{\text{sp}} \int dp p^2 \hat{f}(p) \right] \times \left[\frac{h^2}{\rho_c^0} \right], \quad (10)$$

where $\hat{f}(p)$ is the distribution function as a function of the magnitude of the physical momentum in the conventions

⁴In (5) the convention is that the scale factor is 1 at $\theta = 0$.

of [41].⁵ ρ_c^0 is the critical density today and h the reduced Hubble parameter. In our model, the effective parameters m_{eff} and ΔN_{eff} in terms of the microscopic parameters are given by [37]

$$\Delta N_{\text{eff}} = \frac{43}{7} \frac{B_{\text{sp}}}{1 - B_{\text{sp}}} \left(\frac{g_*(T(t_\nu))}{g_*(T(t^*))} \right)^{1/3} \quad (11)$$

and

$$m_{\text{sp}}^{\text{eff}} = \frac{62.1 m_{\text{sp}}}{g_*^{1/4}(T(t^*))} \frac{B_{\text{sp}}}{(1 - B_{\text{sp}})^{3/4}} \left(\frac{M_{\text{pl}}}{\tau m_\phi^2} \right)^{1/2}, \quad (12)$$

where $g_*(T(t_\nu))$ and $g_*(T(t^*))$ are the effective number of degrees of freedom at the time of neutrino decoupling and the end of the reheating epoch (we will take the latter to be equal to 100). We will thus scan over m_{sp} and B_{sp} (keeping $m_\phi = 10^{-6} M_{\text{pl}}$ and $\tau \sim 10^8/m_\phi$ fixed), and use Eqs. (12) and (11) to relate to phenomenological parameters. See Appendix B for a discussion of a model with a different values of m_ϕ and τ that matches with the above scan when the effective parameters match. In Sec. IV, we will then translate our results for two other models of interest. Note that the free-streaming length can be simply extracted from our analysis using the relation [42]

$$\lambda_{\text{fs}}(t) = 2\pi \sqrt{\frac{2}{3}} \frac{v_s(t)}{H(t)}, \quad (13)$$

where, when evaluated today at $t = t_0$, one has [41]

$$v_s(t_0) \simeq 5.618 \times 10^{-6} \frac{\Delta N_{\text{eff}}}{\omega_s}. \quad (14)$$

III. RESOLVING THE S_8 TENSION WITH A NONTHERMAL STERILE NEUTRINO

A. Details of the analysis

We perform a comprehensive MCMC analysis and confront the nonthermal hot dark matter model to various combination of the following datasets:

- (i) *Planck* 2018 measurements of the low- ℓ CMB temperature correlations power spectra (TT), E mode polarization power spectra (EE), and high- ℓ TT, cross-correlation temperature and E mode polarization power spectra (TE), EE power spectra, together with the gravitational lensing potential reconstruction [1].
- (ii) The BAO measurements from 6dFGS at $z = 0.106$ [56], SDSS DR7 at $z = 0.15$ [57], BOSS DR12 at $z = 0.38, 0.51, \text{ and } 0.61$ [58], and the joint

⁵In these conventions, an additional species of neutrinos at temperature T_s has $\hat{f}(p) = \frac{1}{e^{p/T_s} + 1}$. For our nonthermal distribution $\hat{f}(p) = 4\pi^3 f(\frac{p}{T_{\text{ncdm},0}} \hat{\mathbf{e}})$, where the function f is as defined in (5) and $\hat{\mathbf{e}}$ is an arbitrary unit vector.

constraints from eBOSS DR14 Ly- α autocorrelation at $z = 2.34$ [59] and cross-correlation at $z = 2.35$ [60].

- (iii) The measurements of the growth function $f\sigma_8(z)$ (FS) from the CMASS and LOWZ galaxy samples of BOSS DR12 at $z = 0.38, 0.51, \text{ and } 0.61$ [58].
- (iv) The Pantheon SNIa catalog, spanning redshifts $0.01 < z < 2.3$ [61].
- (v) The KiDS1000 + BOSS + 2dfLenS weak lensing data, compressed as a split-normal likelihood on the parameter $S_8 = 0.766_{-0.014}^{+0.02}$ [7].

Our baseline cosmology consists in the following combination of the six Λ CDM parameters $\{\omega_b, \omega_{\text{cdm}}, 100 \times \theta_s, n_s, \ln(10^{10} A_s), \tau_{\text{reio}}\}$, plus two parameters describing the non-thermal hot dark matter, namely $\{m_{\text{sp}}, B_{\text{sp}}\}$. We dub this model $\nu_{\text{NT}}\Lambda$ CDM. Standard model neutrinos are assumed to be massless.

To better understand how the $\nu_{\text{NT}}\Lambda$ CDM model can resolve the S_8 tension, we will compare it to the standard Λ CDM model with massless neutrinos, as well as to the Λ CDM model with free neutrino masses m_ν and additional relativistic degrees of freedom ΔN_{eff} . In that latter case, we assume degenerate neutrino masses and a free-streaming ΔN_{eff} . Note that in this model, the ΔN_{eff} component does not become massive at late times, contrary to what happens in the non-thermal neutrino model. This will play a key role in the difference between the two models. We dub this model $\nu\Lambda$ CDM. We run our MCMCs with the Metropolis-Hasting algorithm as implemented in the `MontePython-v3` [62] code interfaced with our modified version of `CLASS`. All reported χ_{min}^2 are obtained with the `PYTHON` package `IMINUIT` [63].⁶ We make use of a Choleski decomposition to better handle a large number of nuisance parameters [64] and consider chains to be converged with the Gelman-Rubin convergence criterium $R - 1 \lesssim 0.05$ [65].

B. Results

We run two sets of analysis; in the first one, we confront the Λ CDM, $\nu\Lambda$ CDM, and $\nu_{\text{NT}}\Lambda$ CDM models to *Planck* only and *Planck* + S_8 . In the second one, we add the BAO and Pantheon data to our analysis. Our main results are reported in Tables I and II and displayed on Figs. 2 and 3. We report results in the $\nu_{\text{NT}}\Lambda$ CDM in terms of ΔN_{eff} and $m_{\text{sp}}^{\text{eff}}$ defined in Eqs. (11) and (12). We give the χ_{min}^2 per experiment⁷ in Appendix A.

⁶<https://iminuit.readthedocs.io/>.

⁷Note that we model neutrinos as degenerate in the thermal and non-thermal case, while the Λ CDM model has two massless, and one massive neutrino with $m = 0.06$ eV (following *Planck* convention). This leads to very small differences in practice and explains why we cannot recover exactly the Λ CDM model χ^2 in the massive neutrino cases. Similarly, the nonthermal model does not “exactly” reduce to the thermal model in some part of the parameter space. Small χ^2 differences are therefore expected and safe given their statistical insignificance.

TABLE I. The mean (best-fit) $\pm 1\sigma$ error of the cosmological parameters in the Λ CDM and $\nu_{\text{NT}}\Lambda$ CDM model obtained from the analysis of *Planck* [1] and *Planck* + S_8 [7] data. The definition of $m_{\text{sp}}^{\text{eff}}$ is given in Eq. (12). Upper limits are given at the 95% C.L.

Model	Λ CDM		$\nu\Lambda$ CDM		$\nu_{\text{NT}}\Lambda$ CDM	
	<i>Planck</i>	<i>Planck</i> + S_8	<i>Planck</i>	<i>Planck</i> + S_8	<i>Planck</i>	<i>Planck</i> + S_8
$100\omega_b$	2.24(2.24) $^{+0.014}_{-0.015}$	2.252(2.256) $^{+0.014}_{-0.015}$	2.244 $^{+0.016}_{-0.018}$	2.257(2.259) \pm 0.017	2.241(2.247) $^{+0.015}_{-0.016}$	2.247(2.247) $^{+0.014}_{-0.015}$
ω_{cdm}	0.1198(0.1195) $^{+0.0013}_{-0.0012}$	0.1182(0.1177) \pm 0.0011	0.1217 $^{+0.0015}_{-0.0013}$	0.1198(0.1182) $^{+0.0013}_{-0.0018}$	0.118(0.1198) $^{+0.0041}_{-0.0042}$	0.1142(0.1110) $^{+0.0049}_{-0.0031}$
$100 * \theta_s$	1.04190(1.04178) $^{+0.00029}_{-0.00029}$	1.04202(1.04217) $^{+0.00029}_{-0.0003}$	1.04166 $^{+0.00037}_{-0.00033}$	1.04179(1.04191) $^{+0.00035}_{-0.00032}$	1.04180(1.04187) \pm 0.00032	1.04186(1.04190) $^{+0.00031}_{-0.00029}$
n_s	0.9661(0.9663) $^{+0.0041}_{-0.0043}$	0.9695(0.971) $^{+0.0039}_{-0.0041}$	0.9685 $^{+0.0049}_{-0.006}$	0.9717(0.9732) $^{+0.0048}_{-0.0056}$	0.9652(0.9677) $^{+0.0044}_{-0.0051}$	0.9652(0.9661) $^{+0.0047}_{-0.0045}$
$\ln(10^{10}A_s)$	3.044(3.044) \pm 0.014	3.041(3.042) $^{+0.014}_{-0.015}$	3.052 $^{+0.015}_{-0.016}$	3.048(3.050) $^{+0.016}_{-0.017}$	3.047(3.0480) \pm 0.015	3.046(3.044) $^{+0.014}_{-0.016}$
τ_{reio}	0.0541(0.0541) $^{+0.0075}_{-0.0071}$	0.0542(0.0556) $^{+0.0074}_{-0.0078}$	0.0558 $^{+0.0073}_{-0.0081}$	0.0555(0.0590) $^{+0.0077}_{-0.0082}$	0.0545(0.0559) $^{+0.0073}_{-0.0081}$	0.0548(0.0536) $^{+0.0069}_{-0.0079}$
m_ν (eV)	<0.073	<0.1(0)
$m_{\text{sp}}^{\text{eff}}$ (eV)	<1.02(0)	0.67(0.90) $^{+0.26}_{-0.48}$
ΔN_{eff}	<0.28	<0.24(0.03)	<0.15(0.03)	0.0614(0.034) $^{+0.0052}_{-0.047}$
S_8	0.834(0.832) \pm 0.013	0.814(0.809) $^{+0.011}_{-0.011}$	0.834(0.838) $^{+0.013}_{-0.013}$	0.812(0.814) \pm 0.011	0.815(0.831) $^{+0.022}_{-0.018}$	0.789(0.791) \pm 0.016
Ω_m	0.3078(0.3068) $^{+0.0074}_{-0.0076}$	0.2981(0.2948) $^{+0.0061}_{-0.0066}$	0.3154(0.3084) $^{+0.0094}_{-0.015}$	0.3084(0.295) $^{+0.0081}_{-0.018}$	0.3138(0.305) $^{+0.0084}_{-0.0097}$	0.311(0.308) $^{+0.008}_{-0.01}$
H_0 (km/s/Mpc)	68(68.04) \pm 0.56	68.73(68.99) $^{+0.49}_{-0.51}$	67.83(67.95) $^{+1.2}_{-1}$	68.26(69.11) $^{+1.5}_{-0.93}$	67.72(68.34) $^{+0.62}_{-0.65}$	67.91(68.04) $^{+0.67}_{-0.61}$
χ^2_{min}	2774.8	2783.4	2774.9	2782.0	2775.0	2778.60

TABLE II. Same as Table I with the addition of ‘‘Ext’’ data, which refers to the combination BAO/FS + Pantheon.

Model	Λ CDM		$\nu\Lambda$ CDM		$\nu_{\text{NT}}\Lambda$ CDM	
	<i>Planck</i> + Ext	<i>Planck</i> + Ext + S_8	<i>Planck</i> + Ext	<i>Planck</i> + Ext + S_8	<i>Planck</i> + Ext	<i>Planck</i> + Ext + S_8
$100\omega_b$	2.241(2.238) $^{+0.013}_{-0.014}$	2.248(2.258) \pm 0.013	2.249(2.248) \pm 0.015	2.257(2.250) \pm 0.015	2.245(2.245) \pm 0.014	2.250(2.253) $^{+0.013}_{-0.014}$
ω_{cdm}	0.1197(0.1204) \pm 0.0009	0.1187(0.1182) $^{+0.0009}_{-0.0008}$	0.121(0.1194) $^{+0.0012}_{-0.0019}$	0.1198(0.1186) $^{+0.0011}_{-0.0017}$	0.1181(0.1179) $^{+0.0030}_{-0.0018}$	0.1152(0.1101) $^{+0.0036}_{-0.0023}$
$100 * \theta_s$	1.04192(1.04204) $^{+0.00028}_{-0.00029}$	1.04197(1.04186) $^{+0.0003}_{-0.0003}$	1.04172(1.04194) $^{+0.00034}_{-0.00031}$	1.04179(1.04194) $^{+0.00036}_{-0.00031}$	1.04187(1.04193) $^{+0.0003}_{-0.00029}$	1.04193(1.04194) $^{+0.00029}_{-0.00028}$
n_s	0.9664(0.9660) $^{+0.0038}_{-0.0037}$	0.9683(0.9705) $^{+0.0036}_{-0.0038}$	0.9699(0.9693) $^{+0.0044}_{-0.0049}$	0.9721(0.9706) $^{+0.0043}_{-0.0048}$	0.9667(0.9664) $^{+0.0039}_{-0.0041}$	0.9669(0.9678) $^{+0.0039}_{-0.004}$
$\ln(10^{10}A_s)$	3.044(3.05) $^{+0.014}_{-0.015}$	3.038(3.045) $^{+0.013}_{-0.015}$	3.052(3.049) $^{+0.014}_{-0.016}$	3.046(3.035) $^{+0.015}_{-0.016}$	3.049(3.052) $^{+0.014}_{-0.015}$	3.046(3.054) $^{+0.014}_{-0.015}$
τ_{reio}	0.0542(0.0574) $^{+0.0069}_{-0.0073}$	0.0526(0.056) $^{+0.0069}_{-0.0076}$	0.0561(0.0569) $^{+0.0066}_{-0.0081}$	0.0548(0.0515) $^{+0.0073}_{-0.0081}$	0.0559(0.0576) $^{+0.007}_{-0.0076}$	0.0556(0.0586) $^{+0.0068}_{-0.0076}$
m_ν (eV)	<0.040(0.005)	<0.057(0.01)
$m_{\text{sp}}^{\text{eff}}$ (eV)	<0.67(0.21)	0.48(0.92) $^{+0.17}_{-0.36}$
ΔN_{eff}	<0.27(0.02)	<0.26(0.006)	<0.12(0.02)	0.0457(0.0336) $^{+0.0038}_{-0.031}$
S_8	0.832(0.842) \pm 0.011	0.818(0.815) $^{+0.0091}_{-0.0094}$	0.830(0.827) \pm 0.011	0.814(0.815) $^{+0.01}_{-0.0097}$	0.815(0.820) $^{+0.017}_{-0.015}$	0.795(0.787) $^{+0.015}_{-0.013}$
Ω_m	0.3067(0.31) \pm 0.0055	0.3007(0.2974) $^{+0.0051}_{-0.0049}$	0.3084(0.3042) $^{+0.0059}_{-0.006}$	0.3045(0.3037) $^{+0.0061}_{-0.0072}$	0.309(0.308) $^{+0.0057}_{-0.0061}$	0.306(0.304) \pm 0.006
H_0 (km/s/Mpc)	68.07(67.82) $^{+0.41}_{-0.43}$	68.52(68.78) $^{+0.38}_{-0.4}$	68.35(68.33) $^{+0.56}_{-0.7}$	68.58(68.28) $^{+0.64}_{-0.73}$	68.06(67.97) $^{+0.44}_{-0.47}$	68.22(68.37) $^{+0.41}_{-0.43}$
χ^2_{min}	3810.4	3818.2	3809.5	3816.4	3809.7	3814.5

1. *Planck* only

When the $\nu_{\text{NT}}\Lambda$ CDM model is confronted to *Planck* only, we obtain a bound⁸ on the mass $m_{\text{sp}}^{\text{eff}} < 1.02$ eV and $\Delta N_{\text{eff}} < 0.15$. Similarly, in the $\nu\Lambda$ CDM case we obtain $m_\nu < 0.073$ eV and $\Delta N_{\text{eff}} < 0.28$ (recall that this limit applies to individual neutrino masses in the degenerate case). The χ^2_{min} of *Planck* in the $\nu\Lambda$ CDM and $\nu_{\text{NT}}\Lambda$ CDM scenario is not improved over that of Λ CDM. We note that the $\nu_{\text{NT}}\Lambda$ CDM model predicts a lower S_8 value than other models. Indeed, we find $S_8(\nu\Lambda\text{CDM}) = 0.831^{+0.012}_{-0.013}$ and $S_8(\Lambda\text{CDM}) = 0.832 \pm 0.011$, to be compared to $S_8(\nu_{\text{NT}}\Lambda\text{CDM}) = 0.816^{+0.022}_{-0.016}$, i.e., a $\gtrsim 1\sigma$ downward shift. As a result, the S_8 tension is alleviated from the $\sim 2.7\sigma$ level to the $\sim 1.9\sigma$ level in the nonthermal HDM model. We note

⁸Hereinafter, we quote one-sided constraints at 95% confidence limits (C.L.), and two-sided ones at 68% C.L.

that our constraints on ΔN_{eff} in the nonthermal case is stronger than that reported in Ref. [1] (constraints are identical in the thermal case). This likely comes from the impact of running on physical parameters as opposed to phenomenological parameters when exploring the parameter space.

Including the prior on S_8 , we notice a mild detection of nonzero $m_{\text{sp}}^{\text{eff}} = 0.67^{+0.26}_{-0.48}$ eV and $\Delta N_{\text{eff}} = 0.0614^{+0.0052}_{-0.047}$ in the $\nu_{\text{NT}}\Lambda$ CDM model, while the constraints on the thermal neutrino mass simply relaxes to $m_\nu < 0.1$ eV. This translates into a reconstructed $S_8(\nu_{\text{NT}}\Lambda\text{CDM}) = 0.789 \pm 0.016$ and $S_8(\nu\Lambda\text{CDM}) = 0.812 \pm 0.011$, to be compared with the baseline $S_8(\Lambda\text{CDM}) = 0.814^{+0.01}_{-0.011}$. As a consequence, the χ^2_{min} in the combined analysis is lower in the non-thermal HDM case $\Delta\chi^2_{\text{min}}(\nu_{\text{NT}}\Lambda\text{CDM}) = \chi^2_{\text{min}}(\Lambda\text{CDM}) - \chi^2_{\text{min}}(\nu_{\text{NT}}\Lambda\text{CDM}) = -4.8$ than in the thermal neutrino case $\Delta\chi^2_{\text{min}}(\nu\Lambda\text{CDM}) = \chi^2_{\text{min}}(\Lambda\text{CDM}) - \chi^2_{\text{min}}(\nu\Lambda\text{CDM}) = -1.4$. If the S_8 tension worsens in the future, then it would be

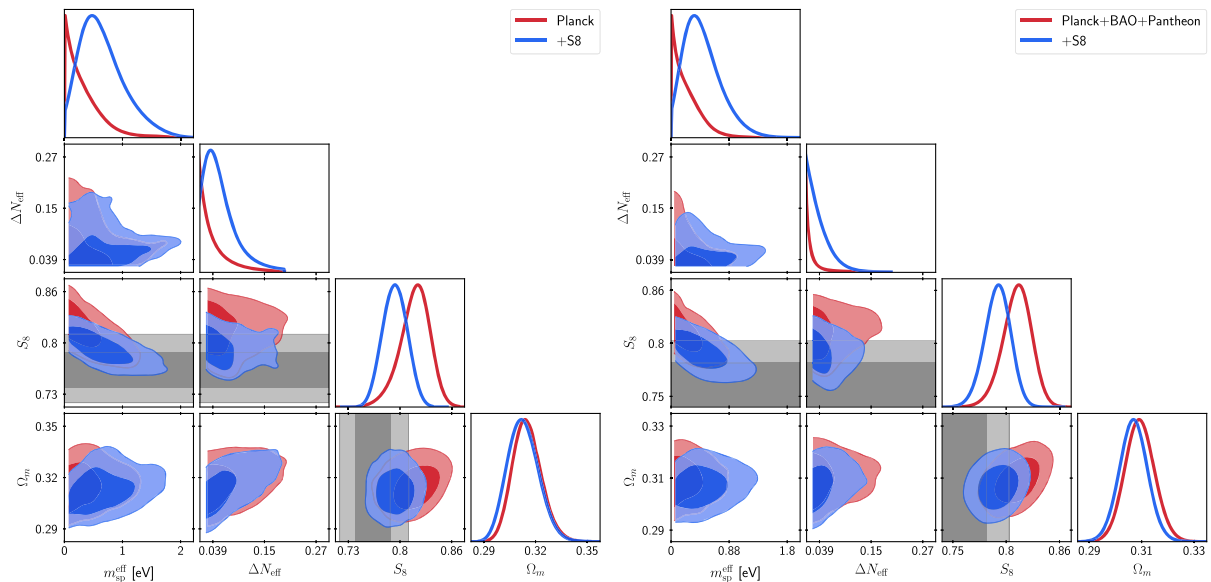


FIG. 2. Reconstructed 2D posterior distributions of $\{m_{\text{sp}}^{\text{eff}}, \Delta N_{\text{eff}}, S_8, \Omega_m\}$ with *Planck* and *Planck* + S_8 data (left panel) or *Planck* + BAO + SNIa and *Planck* + BAO + SNIa + S_8 data (right panel).

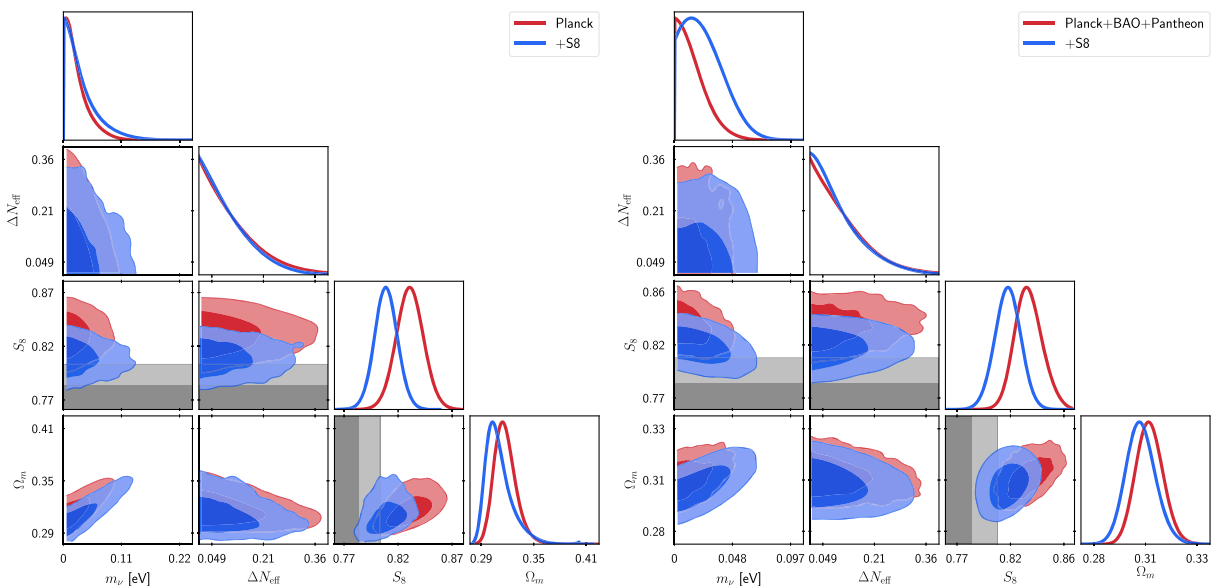


FIG. 3. Same as Fig. 2 in the thermal neutrino case.

interesting to perform a more complete Bayesian analysis comparing these models. We notice, however, that the total χ^2_{min} is much less significantly affected by the inclusion of the S_8 prior in the nonthermal case (+3.6) than in the thermal case (+6.9), which is encouraging and indicates that the $\nu_{\text{NT}}\Lambda\text{CDM}$ model can potentially alleviate the tension between *Planck* and KiDS + BOSS. It remains to be seen whether this is robust to additional datasets (and in the future it should be tested against the full KiDS and BOSS likelihoods).

Before including external data, we comment on the possibility for nonthermal hot dark matter to resolve the

Hubble tension (see, e.g., [66–68] for a review). We find that, whether we include the S_8 prior or not, the value of H_0 is barely affected by the extra ΔN_{eff} (in fact, even shifted slightly towards lower H_0 due to the well-known anti-correlation with $m_{\text{sp}}^{\text{eff}}$ [43]). We, therefore, confirm that these models cannot be responsible for the high- H_0 measured with some of the local probes.

2. *Planck* + BOSS + SNIa

When the BAO/FS and SNIa data are added to the analysis, the constraints on the thermal neutrino mass and

nonthermal hot dark matter mass strengthen. We find $m_{\text{sp}}^{\text{eff}} < 0.67$ eV and $\Delta N_{\text{eff}} < 0.12$ in the $\nu_{\text{NT}}\Lambda\text{CDM}$ model, while we get $m_\nu < 0.04$ eV and $\Delta N_{\text{eff}} < 0.27$ in the thermal case. Still, the reconstructed S_8 value $S_8(\nu_{\text{NT}}\Lambda\text{CDM}) = 0.814^{+0.017}_{-0.014}$ and $S_8(\nu\Lambda\text{CDM}) = 0.83 \pm 0.011$ are slightly smaller than in the Planck-only analysis. This is because the reconstructed value of ω_{cdm} is slightly smaller in the combined analysis with BAO/FS and SNIa data, regardless of the model.

Once the prior on S_8 is added to the analysis, we again find a mild detection of $m_{\text{eff}} = 0.48^{+0.17}_{-0.36}$ eV and $\Delta N_{\text{eff}} = 0.0457^{+0.0038}_{-0.031}$. However, the mean value has decreased by 0.5σ due to the inclusion of BAO/FS and SNIa data. This reflects in a slightly larger reconstructed S_8 value, $S_8(\nu_{\text{NT}}\Lambda\text{CDM}) = 0.795^{+0.015}_{-0.013}$. A similar pattern is observed in the thermal case, for which the relaxation of the constraint to $m_\nu < 0.057$ eV is much milder than without BAO/FS and SNIa data, while the reconstructed

$S_8(\nu\Lambda\text{CDM}) = 0.814 \pm 0.01$ is stable. Looking at χ^2_{min} , one can see that the nonthermal case still provides a better fit $\Delta\chi^2_{\text{min}}(\nu_{\text{NT}}\Lambda\text{CDM}) = -3.7$ than the thermal case $\Delta\chi^2_{\text{min}}(\nu\Lambda\text{CDM}) = -1.8$. However, the inclusion of the S_8 prior as increased the total χ^2_{min} by $+4.8$ in the nonthermal case and $+6.9$ in the thermal case. It is interesting to note that the tension level between *Planck* and KiDS evolves from 1.9σ to 2.2σ once BAO data are included, i.e., these data worsen the tension. This is in contrast with the ΛCDM case, for which the tension goes from 2.9σ (without BAO) to 2.8σ (with BAO). More accurate BAO/FS and SNIa data could therefore pose a serious challenge to this model.

C. Understanding the MCMC

To understand better the results of the MCMC analyses, we show in Fig. 4 the residuals of the CMB TT, EE, lensing (top panel) and matter (bottom panel) power spectra with

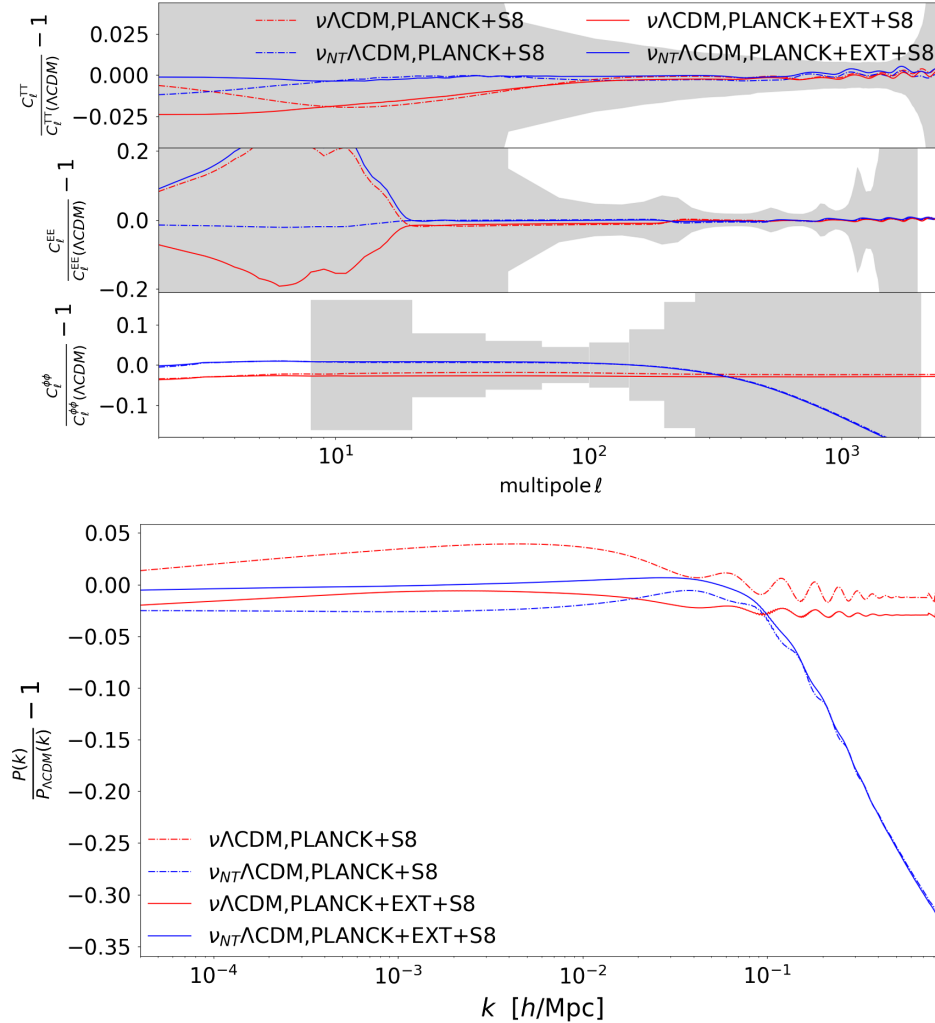


FIG. 4. Residuals of the CMB TT, EE, lensing (top panel) and matter (bottom panel) power spectra with respect to ΛCDM in the best-fit $\nu\Lambda\text{CDM}$ and $\nu_{\text{NT}}\Lambda\text{CDM}$ models for two different datasets (see legend). The “Ext” data refers to BAO/FS + SNIa.

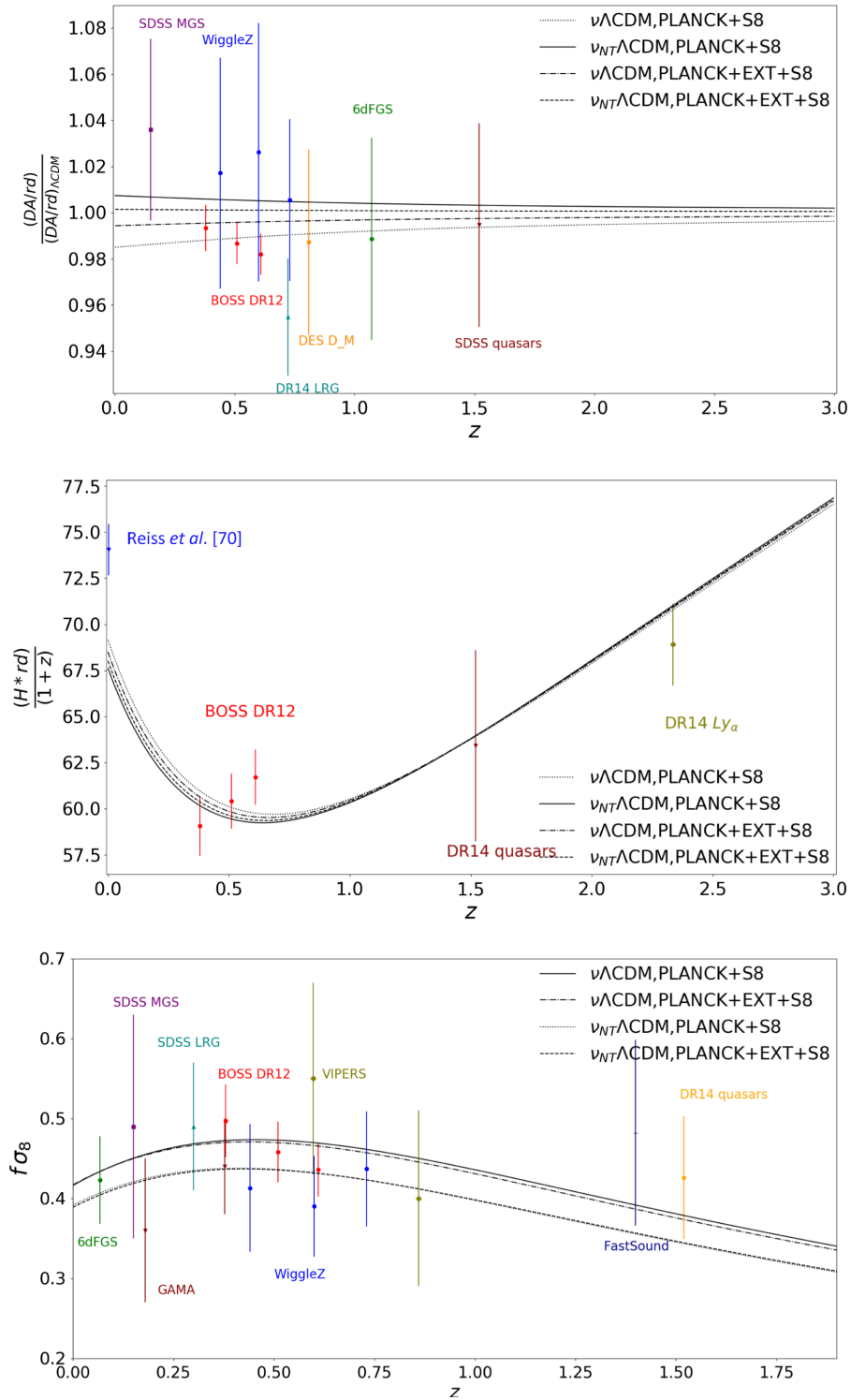


FIG. 5. Transverse BAO (top panel), longitudinal BAO (middle panel), and growth factor (bottom panel) in the best-fit $\nu\Lambda\text{CDM}$ and $\nu_{NT}\Lambda\text{CDM}$ models for two different datasets (see legend). The “Ext” data refers to BAO/FS + SNIa. The transverse BAO has been normalized to the ΛCDM prediction, as in Ref. [69,70].

respect to ΛCDM in the best-fit $\nu\Lambda\text{CDM}$ and $\nu_{NT}\Lambda\text{CDM}$ models obtained when considering *Planck* + *S8* and *Planck* + *Ext* + *S8* data. We also show in Fig. 5 the corresponding transverse BAO (top panel), longitudinal

BAO (middle panel), and growth factor (bottom panel). The first thing to notice is that, for a similar effect in the CMB power spectra, the corresponding power suppression in the matter power spectrum is much stronger in the $\nu_{NT}\Lambda\text{CDM}$

than in the $\nu\Lambda$ CDM model. This is the reason why the $\nu_{\text{NT}}\Lambda$ CDM can perform much better in resolving the S_8 tension.

Looking at the BAO and $f\sigma_8$ prediction, one can see that the most important difference is in the latter, which is significantly lower at all z in the $\nu_{\text{NT}}\Lambda$ CDM because of this power suppression. This explains the small degradation in χ^2 in the combined analysis with S_8 . Moreover, the reconstructed dark matter density ω_{cdm} in the $\nu_{\text{NT}}\Lambda$ CDM is also shifted by roughly $\sim 1\sigma$ downwards (to compensate for the higher energy density due to the nonrelativistic transition of the nonthermal neutrinos), which also leads to a small degradation in the fit to Planck data (hardly visible by eye in CMB power spectra residuals). This small difference in the matter density is also visible in the small $-k$ (large scales) branch of the matter power spectrum, particularly sensitive to Ω_m [71]. While these differences do not yet unambiguously rule out the $\nu_{\text{NT}}\Lambda$ CDM as a resolution to the S_8 tension, they do provide an interesting avenue to probe the model with future data, in particular through accurate measurements of the matter power spectrum, CMB lensing power spectrum and growth factor $f\sigma_8$. A potential way to improve over the $\nu_{\text{NT}}\Lambda$ CDM results presented here is to assume that the hot component comes from the decay of a metastable cold dark matter species in the late Universe [19,20], instead of being present at all times. A good fit to all data can then be obtained when the mass ratio of the mother and daughter particle $\varepsilon \sim 0.007$ and the CDM lifetime $\tau \sim 55$ Gyrs.

IV. IMPLICATIONS FOR OTHER NONTHERMAL HOT DARK MATTER MODELS

As discussed in the introduction and Sec. II B, any distribution with the same values of ΔN_{eff} and $m_{\text{sp}}^{\text{eff}}$ as ours should also relax the σ_8 tension. Our results can thus be used to extract implications for the microscopic parameters of models that have momentum distributions different from the ones we have used. Here, we present such results for two models:

- (i) Sterile particles at a different temperature from that of the Standard Model neutrinos. In this model, sterile neutrinos follow a thermal Fermi-Dirac distribution:

$$\hat{f}(p) = \frac{1}{e^{p/T_s} + 1}, \quad (15)$$

where T_s is the temperature of sterile particles. For a thermal sterile particle with a Fermi-Dirac distribution and a different temperature T_s , the quantities ΔN_{eff} and ω_s become

$$\Delta N_{\text{eff}} = \left(\frac{T_s}{T_{\nu}^{\text{id}}}\right)^4, \quad \omega_s = \frac{m_{\text{sp}}}{94.05} \left(\frac{T_s}{T_{\nu}}\right)^3. \quad (16)$$

TABLE III. Best-fit values of the physical parameters in the nonthermal, thermal, and Dodelson-Widrow sterile neutrino models derived from our analyses.

Model	Nonthermal		Thermal		Dodelson widrow	
	m_{sp} (eV)	B_{sp}	m_{sp} (eV)	$\frac{T_s}{T_{\nu}}$	m_{sp} (eV)	χ
<i>Planck</i>	0.05	0.01	0	0.40	0	0.03
<i>Planck</i> + S_8	38.62	0.012	11.36	0.43	26.43	0.03
<i>Planck</i> + Ext	18.98	0.01	04.59	0.36	12.85	0.02
<i>Planck</i> + Ext + S_8	39.81	0.01	11.75	0.43	27.49	0.03

- (ii) The Dodelson-Widrow distribution [46]

$$\hat{f}(p) = \frac{\chi}{1 + e^{p/T_{\nu}}},$$

where T_{ν} is the temperature of the neutrinos today, χ is a parameter related to the phenomenological parameters as [41],

$$\Delta N_{\text{eff}} = \chi, \quad m_{\text{sp}}^{\text{eff}} = m_{\text{sp}} \times \chi, \quad (17)$$

and m_{sp} is the individual neutrino mass in the model.

We report the best-fit value of the model parameters in Table III, obtained from translating our constraints on ΔN_{eff} and $m_{\text{sp}}^{\text{eff}}$. We also show in Figs. 6 and 7 the residuals of the matter power spectra and CMB, TT, TE, and EE power spectra between our best-fit nonthermal HDM model and these two models. This explicitly demonstrates our claim that, once ΔN_{eff} and $m_{\text{sp}}^{\text{eff}}$ are fixed, observables are indistinguishable. We note that the residuals between the thermal neutrino model at different temperatures and our nonthermal HDM model are of the order of the sensitivity of future LSS experiments such as EUCLID and LSST, and therefore this simple mapping might become limited in the future. Note that, to avoid biasing constraints due to prior effects, we refrain from translating our reconstructed posterior on ΔN_{eff} and $m_{\text{sp}}^{\text{eff}}$ into the model parameters.

The values we report in Table III have direct implication for thermalized hidden sector from both particle physics [72] and cosmological perspective [73,74]. Interestingly the main parameter for building a thermal hidden sector model is the temperature ratio $\xi = \frac{T_s}{T_{\text{vis}}}$ that received a competitive constraint (though it depends on the model) from our analysis and it may have strong implications for light sterile neutrino [73] or other hidden sector particle physics models [75,76]. If the hidden thermal particle interacts with dark matter or other particles in the dark sector, then the coupling and other particle physics parameters can be constrained from our result [77].

It is tantalizing to connect the hot dark matter discussed here to the longstanding (and debated) short base line (SBL) anomalies [78,79] (see [80,81] for recent reviews). Concretely, within the so-called 3 + 1 neutrino scenario,

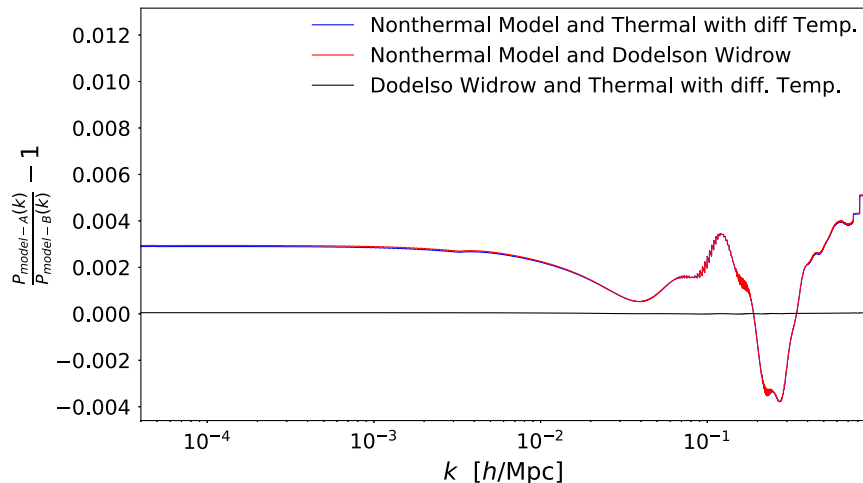
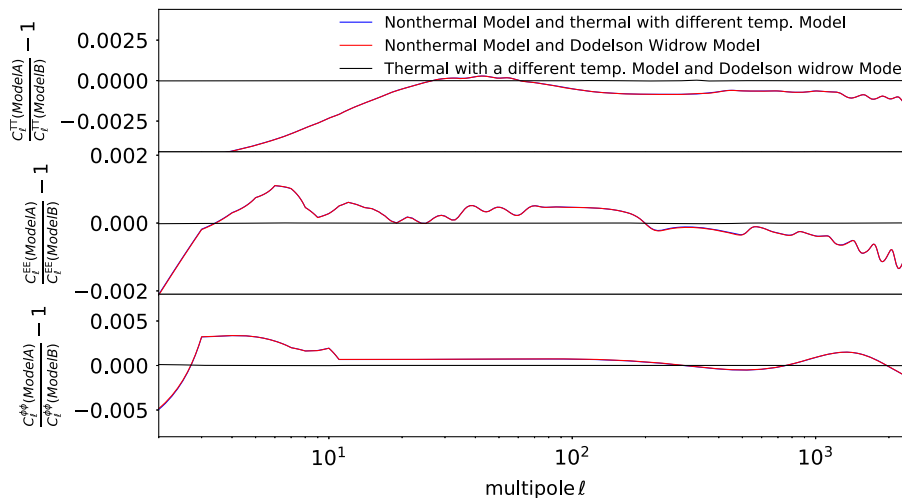


FIG. 6. Residuals of matter power spectra for various models (see legend).


 FIG. 7. Residuals of C_l TT, TE, and EE power spectra for various models (see legend).

those can be explained by a sterile neutrino with $m_s \simeq \sqrt{\Delta m_{41}^2} 1$ eV and a mixing angle leading to $\Delta N_{\text{eff}} \simeq 1$. However, we find that the sterile particles required by the S_8 tension hints to a somewhat higher mass range $m_s \sim \mathcal{O}(10)$ eV (see Table III), and an almost negligible ΔN_{eff} . Our constraints, whether we include the S_8 prior or not, thus further confirm that a viable sterile neutrino solution to the SBL anomalies would require some additional mechanism to prohibit large ΔN_{eff} production (see, e.g., [82–85] for examples). Nevertheless, it could be interesting to perform analysis including results from short baseline neutrino oscillation (e.g., with an additional prior as in Ref. [73]). This is beyond the scope of this paper and is kept for future study.

Finally, we also note that including data from the Bicep2/Keck array [86,87], SPT-3G [88], or ACT [89] could help further constrain the sterile neutrino parameters thanks

to higher accuracy measurement of the CMB damping tail and lensing spectrum. We also keep that for a future study, but refer to Refs. [45,88] for examples (constraints typically increases by $\sim 10\%$, without considering a prior on S_8).

V. DISCUSSION AND CONCLUSIONS

In this paper, we have explored the possibility that the “ S_8 tension,” the long-standing discrepancy between the determination of the amplitude of the matter fluctuations from local [2–7] and cosmological [1] probes, is due to the existence of a nonthermal HDM contributing to a fraction of the DM density in the Universe and leading to a power suppression at small scales in the matter power spectrum. Concretely, we have considered nonthermal HDM produced as decay products of the inflaton. Such particles have the momentum distribution associated with

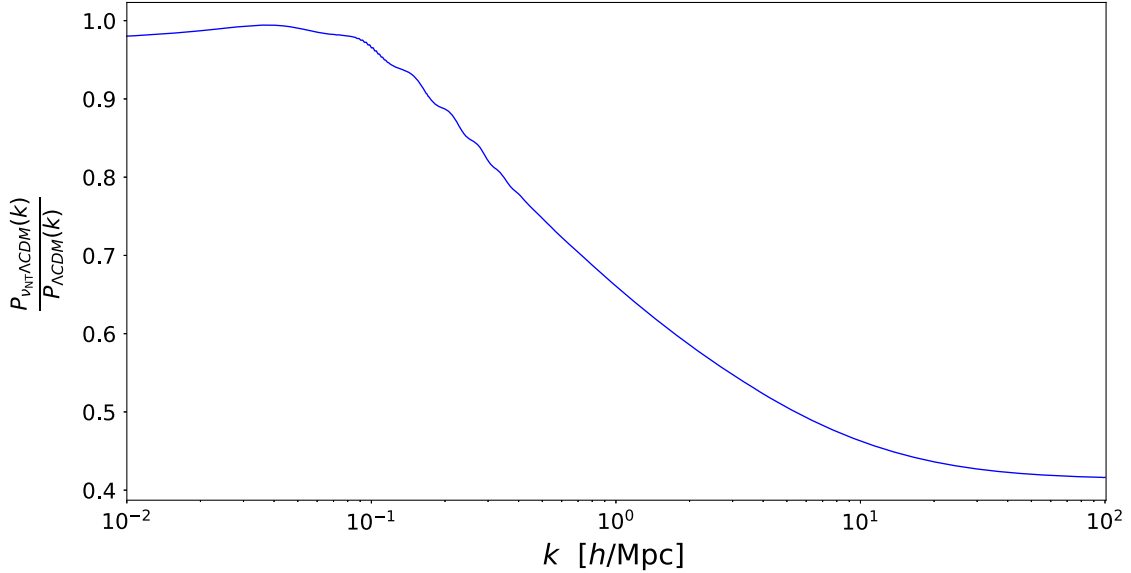


FIG. 8. Ratio of matter power spectra in the $\nu_{\text{NT}}\Lambda\text{CDM}$ model to the ΛCDM model.

decays taking place in a matter-dominated universe evolving to radiation domination, as shown in [37]. However, we have argued that any model leading to the same ΔN_{eff} and $m_{\text{sp}}^{\text{eff}}$ as our model (barring additional new physics ingredients) would lead to similar effects on cosmological observables, and therefore our constraints generically apply to any HDM models.

We have performed a comprehensive MCMC analysis against up-to-date data from *Planck*, BOSS (BAO and $f\sigma_8$), and Pantheon data, with and without the inclusion of a prior on the value of S_8 as measured with the KiDS/Viking + BOSS + 2dFLens data. Our findings can be summarized as follows:

- (1) The $\nu_{\text{NT}}\Lambda\text{CDM}$ model can indeed alleviate the tension between *Planck* and S_8 measurements, but the success of the resolution is degraded once BOSS and Pantheon data are included in the analysis.
- (2) Compared to standard thermal neutrinos, the $\nu_{\text{NT}}\Lambda\text{CDM}$ leads to a much stronger suppression in the matter power spectrum at late times for a similar effect on the CMB power spectrum, and therefore to a more significant decrease in σ_8 .
- (3) The impact of the $\nu_{\text{NT}}\Lambda\text{CDM}$ is barely visible on the BAO scale and luminosity distance, but it does affect $f\sigma_8$ predictions. The model is, therefore, constrained by current BOSS growth factor measurements, and future measurements of the matter power spectrum and $f\sigma_8$ at late times will further test this scenario.
- (4) We further discussed the connection between our model and generic phenomenological parameters

constrained by the data that can be easily used to translate our constraints onto other similar models. Especially, we put constraints on other nonthermal HDM models—like the Dodelson-Widrow models or on a thermal sterile particle with a different temperature in the hidden sector. We report competitive constraints on the hidden sector temperature and DW scaling parameter which can have interesting particle physics implications, for instance in the context of SBL anomalies [78–81].

It will be interesting to confront this model to Lyman- α forest flux power spectrum data along the lines of recent works [10,34,90–95]. For instance, Ref. [93] established that any noncold DM scenario must leave the spectrum at $k \lesssim 33 h/\text{Mpc}$ unaffected. The model studied, whose spectrum shows deviation already at $k \sim 0.05\text{--}1 h/\text{Mpc}$, could therefore likely be probed by Lyman- α data. Nevertheless, the nonthermal neutrino only represents a small fraction of the total DM density, and constraints do not necessarily trivially apply on the model, since the suppression stops at large ks . This is explicitly shown in Fig. 8, where we compare the linear prediction of the matter power spectrum for the ΛCDM and $\nu_{\text{NT}}\Lambda\text{CDM}$ model at scales up to $k = 100 h/\text{Mpc}$. For instance, Ref. [96] derived constraints on WDM + CDM models, showing that model with similar level of suppression at high ks than the one studied here are allowed by the data (although an analysis of more recent data is still lacking). Additionally, the latest study dealing with thermal warm dark matter and neutrinos, has established a mild tension (3σ) between Lyman- α and

Planck data [94]. In the context of the σ_8 tension, it would therefore be interesting to check in detail whether a nonthermal hot dark matter model can play a role in alleviating the “lyman- α tension.”⁹ Additionally, future high accuracy measurement of the matter power spectrum at small scales by upcoming surveys such as Euclid [98], LSST [99], and DESI [100] can further test these models as a resolution to the S_8 tension.

ACKNOWLEDGMENTS

We thank Guillermo Franco Abellàn and Riccardo Murgia for many interesting discussions. We thank the anonymous referee for useful comments that helped improve our paper. A. M. is supported in part by the SERB, DST, Government of India by Grant No. MTR/2019/000267. S. D. acknowledges the SERB, DST Government of India Grant No. CRG/2019/006147 for supporting the project. V. P. is partly supported by the CNRS-IN2P3 Grant No. Dark21 and by the European Union’s Horizon 2020 research and innovation program under the Marie Skłodowska-Curie Grant Agreement No. 860881-HIDDeN. The authors acknowledge the use of computational resources from the Dark Energy computing Center funded by the OCEVU Labex (ANR-11-LABX-0060) and the Excellence Initiative of Aix-Marseille University (A*MIDEX) of the “Investissements d’Avenir” programme as well as IIA Nova cluster where initial analysis was carried out.

APPENDIX A: χ^2_{\min} PER EXPERIMENT

We report χ^2_{\min} per experiment in each of the analysis performed in Tables IV–VI.

⁹We note that approximate bounds could be computed using a formalism relating the constraints on effective parameters between models (see, e.g., Ref. [97]). However, this would be missing the possibility that the model helps in resolving the tension, and therefore it is worth looking into it in more details than this matching.

TABLE IV. Best-fit χ^2 per experiment (and total) in the Λ CDM model.

Experiment	Λ CDM			
<i>Planck</i> high- ℓ TT,TE,EE	2346.7	2350.8	2346	2349.1
<i>Planck</i> low- ℓ EE	396	396.1	396.8	396.2
<i>Planck</i> low- ℓ TT	23.2	22.5	23.4	22.6
<i>Planck</i> lensing	8.8	9.6	9.2	9.1
Pantheon	1026.9	1026.7
BAO/FS BOSS DR12	6.9	6.5
BAO BOSS low- z	1.2	2.3
KiDS/BOSS/2dFGS	...	4.6	...	5.9
Total	2774.8	2783.4	3810.4	3818.2

TABLE V. Best-fit χ^2 per experiment (and total) in the model with massive thermal neutrinos and additional relativistic degrees of freedom.

Experiment	$\nu\Lambda$ CDM			
<i>Planck</i> high- ℓ TT,TE,EE	2345.98	2348.2	2346.9	2348.6
<i>Planck</i> low- ℓ EE	396.54	396.8	396.5	395.7
<i>Planck</i> low- ℓ TT	23.3	22.2	22.8	22.4
<i>Planck</i> lensing	9.03	8.9	8.8	9.3
Pantheon	1026.8	1026.7
BAO/FS BOSS DR12	6.1	5.9
BAO BOSS low- z	1.7	1.7
KiDS/BOSS/2dFGS	...	5.8	...	6.1
Total	2774.9	2782.0	3809.5	3816.4

TABLE VI. Best-fit χ^2 per experiment (and total) in the nonthermal sterile neutrino model.

Experiment	$\nu_{\text{NT}}\Lambda$ CDM			
<i>Planck</i> high- ℓ TT,TE,EE	2346.7	2348.7	2346.4	2349.1
<i>Planck</i> low- ℓ EE	396.3	395.9	396.8	396.9
<i>Planck</i> low- ℓ TT	23.1	23.3	23.4	23.1
<i>Planck</i> lensing	8.8	9.2	8.8	9.1
Pantheon	1026.8	1026.7
BAO/FS BOSS DR12	6.1	6.8
BAO BOSS low- z	1.4	1.7
KiDS/BOSS/2dFGS	...	1.6	...	1.2
Total	2775.0	2778.6	3809.7	3814.5

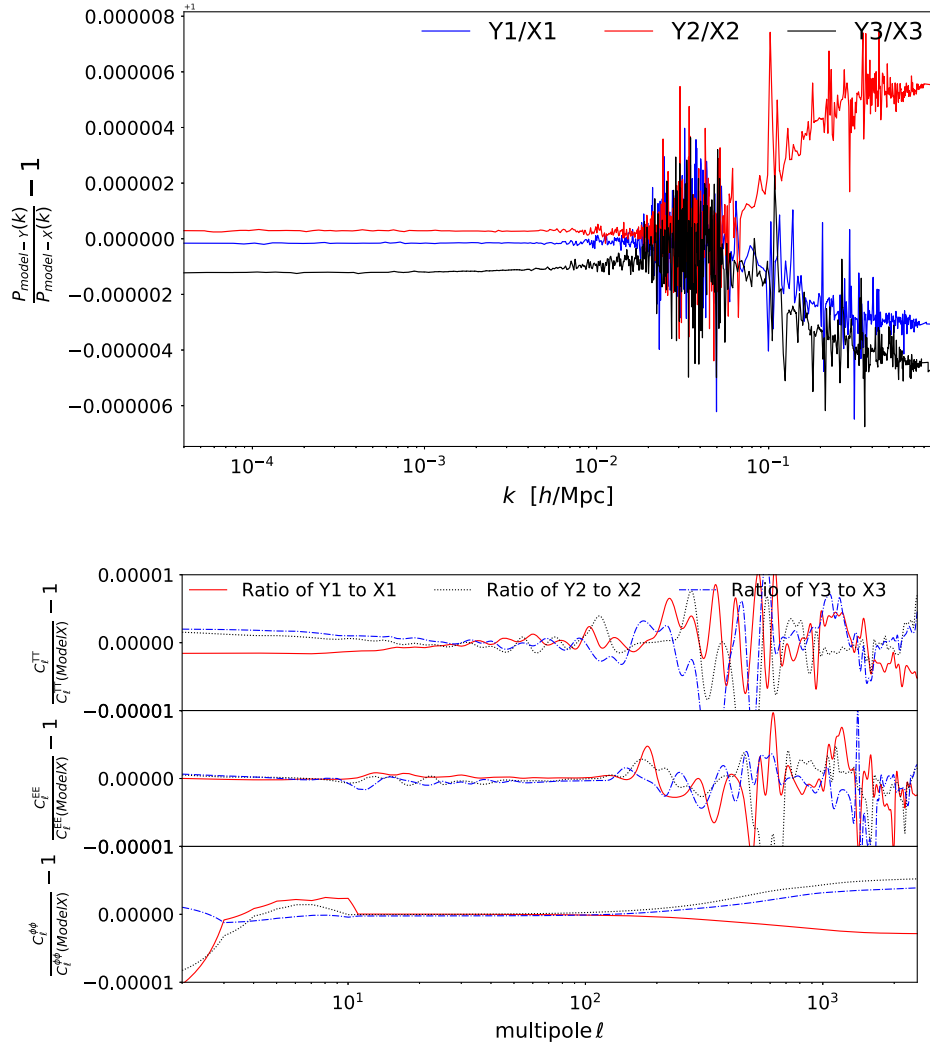


FIG. 9. Residuals of matter power spectra and CMB TT EE $\phi\phi$ power spectra for various models (see legend). Here the models (X1,Y1),(X2,Y2),(X3,Y3) correspond to the models described in Table VII.

APPENDIX B: ON THE RELATIONSHIP BETWEEN OBSERVABLES AND EFFECTIVE PARAMETERS

The fact that the two parameters ΔN_{eff} and m_{eff} determine the physical observables is well known, as mentioned already [41]. In fact, this is also used by the Planck collaboration for their analysis, see, e.g., Fig. 37,

Sec. 7.5.2 of [101]. For completeness, in this appendix we analyze this expectation in our setting. In the model discussed in the main text $m_\phi = 10^{-6}M_{\text{pl}}$ and $\tau = 10^8/m_\phi$ (we will refer to this as model X). Here, we consider $m_\phi = 10^{-8}M_{\text{pl}}$ and $\tau = 10^9/m_\phi$ (we will refer to this as model Y).

Note that Eqs. (11) and (12) imply that if $B_{\text{sp}}^Y = B_{\text{sp}}^X$ and $m_{\text{sp}}^Y = m_{\text{sp}}^X/\sqrt{10}$, models X and Y will have equal values of

TABLE VII. Table shows the parameters of three pairs of model (X1,Y1),(X2,Y2),(X3,Y3). Both the models of the each pair have different values of τ and m_ϕ .

Parameter	Model X1	Model Y1	Model X2	Model Y2	Model X3	Model Y3
m_ϕ	$10^{-6}M_{\text{pl}}$	$10^{-8}M_{\text{pl}}$	$10^{-6}M_{\text{pl}}$	$10^{-8}M_{\text{pl}}$	$10^{-6}M_{\text{pl}}$	$10^{-8}M_{\text{pl}}$
τ	$10^8/m_\phi$	$10^9/M_\phi$	$10^8/m_\phi$	$10^9/m_\phi$	$10^8/m_\phi$	$10^9/m_\phi$
m_{sp} (in eV)	38.62194	$\frac{38.62194}{\sqrt{10}}$	38.62194	$\frac{38.62194}{\sqrt{10}}$	28.62194	$\frac{28.62194}{\sqrt{10}}$
B_{sp}	0.0118	0.0118	0.0218	0.0218	0.0218	0.0218

ΔN_{eff} and m_{eff} . We compare the CMB and matter power spectra today for equal values of m_{sp} and B_{sp} in Fig. 9. As expected, we find that the CLASS inputs of models X and Y

are in very good agreement (better than 10^{-5}). Therefore, our constraints are robust to the specific choice of these parameters.

-
- [1] N. Aghanim *et al.* (Planck Collaboration), Planck 2018 results. VI. Cosmological parameters, [arXiv:1807.06209](https://arxiv.org/abs/1807.06209).
- [2] C. Heymans *et al.*, CFHTLenS tomographic weak lensing cosmological parameter constraints: Mitigating the impact of intrinsic galaxy alignments, *Mon. Not. R. Astron. Soc.* **432**, 2433 (2013).
- [3] N. MacCrann, J. Zuntz, S. Bridle, B. Jain, and M. R. Becker, Cosmic discordance: Are planck CMB and CFHTLenS weak lensing measurements out of tune?, *Mon. Not. R. Astron. Soc.* **451**, 2877 (2015).
- [4] H. Hildebrandt *et al.*, KiDS + VIKING-450: Cosmic shear tomography with optical and infrared data, *Astron. Astrophys.* **633**, A69 (2020).
- [5] S. Joudaki *et al.*, KiDS + VIKING-450 and DES-Y1 combined: Cosmology with cosmic shear, *Astron. Astrophys.* **638**, L1 (2020).
- [6] T. Abbott *et al.* (DES Collaboration), Dark energy survey year 1 results: Cosmological constraints from galaxy clustering and weak lensing, *Phys. Rev. D* **98**, 043526 (2018).
- [7] C. Heymans *et al.*, KiDS-1000 cosmology: Multi-probe weak gravitational lensing and spectroscopic galaxy clustering constraints, *Astron. Astrophys.* **646**, A140 (2021).
- [8] S. Kumar and R. C. Nunes, Probing the interaction between dark matter and dark energy in the presence of massive neutrinos, *Phys. Rev. D* **94**, 123511 (2016).
- [9] R. Murgia, S. Gariazzo, and N. Fornengo, Constraints on the coupling between dark energy and dark matter from CMB data, *J. Cosmol. Astropart. Phys.* **04** (2016) 014.
- [10] M. Archidiacono, D. C. Hooper, R. Murgia, S. Bohr, J. Lesgourgues, and M. Viel, Constraining dark matter-dark radiation interactions with CMB, BAO, and Lyman- α , *J. Cosmol. Astropart. Phys.* **10** (2019) 055.
- [11] E. Di Valentino *et al.*, Cosmology intertwined III: $f\sigma_8$ and S_8 , [arXiv:2008.11285](https://arxiv.org/abs/2008.11285).
- [12] N. Becker, D. C. Hooper, F. Kahlhoefer, J. Lesgourgues, and N. Schöneberg, Cosmological constraints on multi-interacting dark matter, *J. Cosmol. Astropart. Phys.* **02** (2021) 019.
- [13] K. Enqvist, S. Nadathur, T. Sekiguchi, and T. Takahashi, Decaying dark matter and the tension in σ_8 , *J. Cosmol. Astropart. Phys.* **09** (2015) 067.
- [14] V. Poulin, P. D. Serpico, and J. Lesgourgues, A fresh look at linear cosmological constraints on a decaying Dark Matter component, *J. Cosmol. Astropart. Phys.* **08** (2016) 036.
- [15] K. Vattis, S. M. Koushiappas, and A. Loeb, Dark matter decaying in the late Universe can relieve the H_0 tension, *Phys. Rev. D* **99**, 121302 (2019).
- [16] B. S. Haridasu and M. Viel, Late-time decaying dark matter: Constraints and implications for the H_0 -tension, *Mon. Not. R. Astron. Soc.* **497**, 1757 (2020).
- [17] S. J. Clark, K. Vattis, and S. M. Koushiappas, Cosmological constraints on late-Universe decaying dark matter as a solution to the H_0 tension, *Phys. Rev. D* **103**, 043014 (2021).
- [18] K. L. Pandey, T. Karwal, and S. Das, Alleviating the H_0 and σ_8 anomalies with a decaying dark matter model, *J. Cosmol. Astropart. Phys.* **07** (2020) 026.
- [19] G. F. Abellan, R. Murgia, V. Poulin, and J. Lavalle, Hints for decaying dark matter from S_8 measurements, [arXiv:2008.09615](https://arxiv.org/abs/2008.09615).
- [20] G. F. Abellán, R. Murgia, and V. Poulin, Linear cosmological constraints on 2-body decaying dark matter scenarios and robustness of the resolution to the S_8 tension, *Phys. Rev. D* **104**, 123533 (2021).
- [21] V. Poulin, K. K. Boddy, S. Bird, and M. Kamionkowski, Implications of an extended dark energy cosmology with massive neutrinos for cosmological tensions, *Phys. Rev. D* **97**, 123504 (2018).
- [22] C. D. Kreisch, F.-Y. Cyr-Racine, and O. Doré, The neutrino puzzle: Anomalies, interactions, and cosmological tensions, *Phys. Rev. D* **101**, 123505 (2020).
- [23] G. Kane, K. Sinha, and S. Watson, Cosmological moduli and the post-inflationary universe: A critical review, *Int. J. Mod. Phys. D* **24**, 1530022 (2015).
- [24] L. Kofman, A. D. Linde, and A. A. Starobinsky, Towards the theory of reheating after inflation, *Phys. Rev. D* **56**, 3258 (1997).
- [25] R. Allahverdi, R. Brandenberger, F.-Y. Cyr-Racine, and A. Mazumdar, Reheating in inflationary cosmology: Theory and applications, *Annu. Rev. Nucl. Part. Sci.* **60**, 27 (2010).
- [26] A. Berlin, D. Hooper, and G. Krnjaic, Thermal dark matter from a highly decoupled sector, *Phys. Rev. D* **94**, 095019 (2016).
- [27] T. Tenkanen and V. Vaskonen, Reheating the Standard Model from a hidden sector, *Phys. Rev. D* **94**, 083516 (2016).
- [28] G. D. Coughlan, W. Fischler, E. W. Kolb, S. Raby, and G. G. Ross, Cosmological problems for the polyni potential, *Phys. Lett.* **131B**, 59 (1983).
- [29] T. Banks, D. B. Kaplan, and A. E. Nelson, Cosmological implications of dynamical supersymmetry breaking, *Phys. Rev. D* **49**, 779 (1994).
- [30] B. de Carlos, J. A. Casas, F. Quevedo, and E. Roulet, Model independent properties and cosmological implications of the dilaton and moduli sectors of 4-d strings, *Phys. Lett. B* **318**, 447 (1993).

- [31] L. Randall and S. D. Thomas, Solving the cosmological moduli problem with weak scale inflation, *Nucl. Phys.* **B449**, 229 (1995).
- [32] M. Cicoli, K. Dutta, A. Maharana, and F. Quevedo, Moduli vacuum misalignment and precise predictions in string inflation, *J. Cosmol. Astropart. Phys.* **08** (2016) 006.
- [33] B. S. Acharya, M. Dhuria, D. Ghosh, A. Maharana, and F. Muia, Cosmology in the presence of multiple light moduli, *J. Cosmol. Astropart. Phys.* **11** (2019) 035.
- [34] C. Miller, A. L. Erickcek, and R. Murgia, Constraining nonthermal dark matter's impact on the matter power spectrum, *Phys. Rev. D* **100**, 123520 (2019).
- [35] R. J. Scherrer and M. S. Turner, Primordial nucleosynthesis with decaying particles. 1. Entropy producing decays. 2. Inert decays, *Astrophys. J.* **331**, 19 (1988).
- [36] J. Hasenkamp and J. Kersten, Dark radiation from particle decay: Cosmological constraints and opportunities, *J. Cosmol. Astropart. Phys.* **08** (2013) 024.
- [37] S. Bhattacharya, S. Das, K. Dutta, M. R. Gangopadhyay, R. Mahanta, and A. Maharana, Non-thermal hot dark matter from inflaton/moduli decay: The momentum distribution and relaxing the cosmological mass bound, *Phys. Rev. D* **103**, 063503 (2021).
- [38] A. Boyarsky, M. Ovchinnikov, N. Sabti, and V. Syvolap, When FIMPs decay into neutrinos: The N_{eff} story, *Phys. Rev. D* **104**, 035006 (2021).
- [39] Z. Hou, R. Keisler, L. Knox, M. Millea, and C. Reichardt, How massless neutrinos affect the cosmic microwave background damping tail, *Phys. Rev. D* **87**, 083008 (2013).
- [40] J. P. Conlon and M. C. D. Marsh, The cosmophenomenology of axionic dark radiation, *J. High Energy Phys.* **10** (2013) 214.
- [41] M. A. Acero and J. Lesgourgues, Cosmological constraints on a light non-thermal sterile neutrino, *Phys. Rev. D* **79**, 045026 (2009).
- [42] J. Lesgourgues and S. Pastor, Massive neutrinos and cosmology, *Phys. Rep.* **429**, 307 (2006).
- [43] J. Lesgourgues, The cosmic linear anisotropy solving system (CLASS) I: Overview, [arXiv:1104.2932](https://arxiv.org/abs/1104.2932).
- [44] S. Roy Choudhury and S. Hannestad, Updated results on neutrino mass and mass hierarchy from cosmology with Planck 2018 likelihoods, *J. Cosmol. Astropart. Phys.* **07** (2020) 037.
- [45] S. Roy Choudhury and S. Choubey, Constraining light sterile neutrino mass with the BICEP2/Keck Array 2014 B-mode polarization data, *Eur. Phys. J. C* **79**, 557 (2019).
- [46] S. Dodelson and L. M. Widrow, Sterile Neutrinos as Dark Matter, *Phys. Rev. Lett.* **72**, 17 (1994).
- [47] D. Benisty, Quantifying the S_8 tension with the Redshift Space Distortion data set, *Phys. Dark Universe* **31**, 100766 (2021).
- [48] A. Cuoco, J. Lesgourgues, G. Mangano, and S. Pastor, Do observations prove that cosmological neutrinos are thermally distributed?, *Phys. Rev. D* **71**, 123501 (2005).
- [49] J. L. Feng, H. Tu, and H.-B. Yu, Thermal relics in hidden sectors, *J. Cosmol. Astropart. Phys.* **10** (2008) 043.
- [50] S. Das and K. Sigurdson, Cosmological limits on hidden sector dark matter, *Phys. Rev. D* **85**, 063510 (2012).
- [51] S. Das, R. Mondal, V. Rentala, and S. Suresh, On dark matter—dark radiation interaction and cosmic reionization, *J. Cosmol. Astropart. Phys.* **08** (2018) 045.
- [52] A. Berlin, N. Blinov, and S. W. Li, Dark sector equilibration during nucleosynthesis, *Phys. Rev. D* **100**, 015038 (2019).
- [53] G. Gelmini, S. Palomares-Ruiz, and S. Pascoli, Low Reheating Temperature and the Visible Sterile Neutrino, *Phys. Rev. Lett.* **93**, 081302 (2004).
- [54] G. Gelmini, E. Osoba, S. Palomares-Ruiz, and S. Pascoli, MeV sterile neutrinos in low reheating temperature cosmological scenarios, *J. Cosmol. Astropart. Phys.* **10** (2008) 029.
- [55] J. Lesgourgues and T. Tram, The Cosmic Linear Anisotropy Solving System (CLASS) IV: Efficient implementation of non-cold relics, *J. Cosmol. Astropart. Phys.* **09** (2011) 032.
- [56] F. Beutler, C. Blake, M. Colless, D. H. Jones, L. Staveley-Smith, L. Campbell, Q. Parker, W. Saunders, and F. Watson, The 6dF galaxy survey: Baryon acoustic oscillations and the local Hubble constant, *Mon. Not. R. Astron. Soc.* **416**, 3017 (2011).
- [57] A. J. Ross, L. Samushia, C. Howlett, W. J. Percival, A. Burden, and M. Manera, The clustering of the SDSS DR7 main Galaxy sample—I. A 4 per cent distance measure at $z = 0.15$, *Mon. Not. R. Astron. Soc.* **449**, 835 (2015).
- [58] S. Alam *et al.* (BOSS Collaboration), The clustering of galaxies in the completed SDSS-III Baryon Oscillation Spectroscopic Survey: Cosmological analysis of the DR12 galaxy sample, *Mon. Not. R. Astron. Soc.* **470**, 2617 (2017).
- [59] V. de Sainte Agathe *et al.*, Baryon acoustic oscillations at $z = 2.34$ from the correlations of Ly α absorption in eBOSS DR14, *Astron. Astrophys.* **629**, A85 (2019).
- [60] M. Blomqvist *et al.*, Baryon acoustic oscillations from the cross-correlation of Ly α absorption and quasars in eBOSS DR14, *Astron. Astrophys.* **629**, A86 (2019).
- [61] D. M. Scolnic *et al.*, The complete light-curve sample of spectroscopically confirmed SNe Ia from Pan-STARRS1 and cosmological constraints from the combined pantheon sample, *Astrophys. J.* **859**, 101 (2018).
- [62] T. Brinckmann and J. Lesgourgues, MontePython 3: Boosted MCMC sampler and other features, *Phys. Dark Universe* **24**, 100260 (2019).
- [63] F. James and M. Roos, Minuit—a system for function minimization and analysis of the parameter errors and correlations, *Comput. Phys. Commun.* **10**, 343 (1975).
- [64] A. Lewis, A. Challinor, and A. Lasenby, Efficient computation of CMB anisotropies in closed FRW models, *Astrophys. J.* **538**, 473 (2000).
- [65] A. Gelman and D. B. Rubin, Inference from iterative simulation using multiple sequences, *Stat. Sci.* **7**, 457 (1992).
- [66] A. G. Riess, S. Casertano, W. Yuan, J. B. Bowers, L. Macri, J. C. Zinn, and D. Scolnic, Cosmic distances calibrated to 1% precision with Gaia EDR3 parallaxes and Hubble Space Telescope photometry of 75 Milky Way Cepheids confirm tension with Λ CDM, *Astrophys. J. Lett.* **908**, L6 (2021).

- [67] W. L. Freedman, B. F. Madore, T. Hoyt, I. S. Jang, R. Beaton, M. G. Lee, A. Monson, J. Neeley, and J. Rich, Calibration of the tip of the red giant branch (TRGB), *Astrophys. J.* **891**, 57 (2020).
- [68] E. Di Valentino, O. Mena, S. Pan, L. Visinelli, W. Yang, A. Melchiorri, D. F. Mota, A. G. Riess, and J. Silk, In the realm of the Hubble tension—a review of solutions, *Classical Quantum Gravity* **38**, 153001 (2021).
- [69] N. Aghanim *et al.* (Planck Collaboration), Planck 2018 results. I. Overview and the cosmological legacy of Planck, *Astron. Astrophys.* **641**, A1 (2020).
- [70] A. G. Riess, S. Casertano, W. Yuan, L. M. Macri, and D. Scolnic, Large Magellanic Cloud Cepheid Standards provide a 1% foundation for the determination of the Hubble constant and stronger evidence for physics beyond Λ CDM, *Astrophys. J.* **876**, 85 (2019).
- [71] J. Lesgourgues, G. Mangano, G. Miele, and S. Pastor, *Neutrino Cosmology* (Cambridge University Press, Cambridge, England, 2013).
- [72] M. Reece and T. Roxlo, Nonthermal production of dark radiation and dark matter, *J. High Energy Phys.* **09** (2016) 096.
- [73] S. Gariazzo, C. Giunti, and M. Laveder, Light sterile neutrinos in cosmology and short-baseline oscillation experiments, *J. High Energy Phys.* **11** (2013) 211.
- [74] F.-Y. Cyr-Racine, R. de Putter, A. Raccanelli, and K. Sigurdson, Constraints on large-scale dark acoustic oscillations from cosmology, *Phys. Rev. D* **89**, 063517 (2014).
- [75] R. Foot, Mirror dark matter: Cosmology, galaxy structure and direct detection, *Int. J. Mod. Phys. A* **29**, 1430013 (2014).
- [76] U. França, R. A. Lineros, J. Palacio, and S. Pastor, Probing interactions within the dark matter sector via extra radiation contributions, *Phys. Rev. D* **87**, 123521 (2013).
- [77] C. Brust, D. E. Kaplan, and M. T. Walters, New light species and the CMB, *J. High Energy Phys.* **12** (2013) 058.
- [78] A. Aguilar-Arevalo *et al.* (LSND Collaboration), Evidence for neutrino oscillations from the observation of $\bar{\nu}_e$ appearance in a $\bar{\nu}_\mu$ beam, *Phys. Rev. D* **64**, 112007 (2001).
- [79] A. A. Aguilar-Arevalo *et al.* (MiniBooNE Collaboration), Improved Search for $\bar{\nu}_\mu \rightarrow \bar{\nu}_e$ Oscillations in the MiniBooNE Experiment, *Phys. Rev. Lett.* **110**, 161801 (2013).
- [80] J. Kopp, P. A. N. Machado, M. Maltoni, T. Schwetz, Sterile neutrino oscillations: The global picture, *J. High Energy Phys.* **05** (2013) 050.
- [81] M. Dentler, A. Hernández-Cabezudo, J. Kopp, P. A. N. Machado, M. Maltoni, I. Martinez-Soler, and T. Schwetz, Updated global analysis of neutrino oscillations in the presence of eV-Scale sterile neutrinos, *J. High Energy Phys.* **08** (2018) 010.
- [82] J. Hamann, S. Hannestad, G. G. Raffelt, and Y. Y. Y. Wong, Sterile neutrinos with eV masses in cosmology: How disfavoured exactly?, *J. Cosmol. Astropart. Phys.* **09** (2011) 034.
- [83] M. Archidiacono, S. Gariazzo, C. Giunti, S. Hannestad, R. Hansen, M. Laveder, and T. Tram, Pseudoscalar—sterile neutrino interactions: Reconciling the cosmos with neutrino oscillations, *J. Cosmol. Astropart. Phys.* **08** (2016) 067.
- [84] X. Chu, B. Dasgupta, and J. Kopp, Sterile neutrinos with secret interactions—lasting friendship with cosmology, *J. Cosmol. Astropart. Phys.* **10** (2015) 011.
- [85] P. F. de Salas, M. Lattanzi, G. Mangano, G. Miele, S. Pastor, and O. Pisanti, Bounds on very low reheating scenarios after Planck, *Phys. Rev. D* **92**, 123534 (2015).
- [86] P. A. R. Ade *et al.* (BICEP2, Keck Array Collaborations), Improved Constraints on Cosmology and Foregrounds from BICEP2 and Keck Array Cosmic Microwave Background Data with Inclusion of 95 GHz Band, *Phys. Rev. Lett.* **116**, 031302 (2016).
- [87] P. A. R. Ade *et al.* (BICEP2, Keck Array Collaborations), BICEP2/Keck Array x: Constraints on Primordial Gravitational Waves using Planck, WMAP, and New BICEP2/Keck Observations through the 2015 Season, *Phys. Rev. Lett.* **121**, 221301 (2018).
- [88] L. Balkenhol *et al.* (SPT Collaboration), Constraints on Λ CDM extensions from the SPT-3G 2018 EE and TE power spectra, *Phys. Rev. D* **104**, 083509 (2021).
- [89] S. Aiola *et al.* (ACT Collaboration), The atacama cosmology telescope: DR4 maps and cosmological parameters, *J. Cosmol. Astropart. Phys.* **12** (2020) 047.
- [90] M.-Y. Wang, R. A. C. Croft, A. H. G. Peter, A. R. Zentner, and C. W. Purcell, Lyman- α forest constraints on decaying dark matter, *Phys. Rev. D* **88**, 123515 (2013).
- [91] R. Murgia, A. Merle, M. Viel, M. Totzauer, and A. Schneider, “Non-cold” dark matter at small scales: A general approach, *J. Cosmol. Astropart. Phys.* **11** (2017) 046.
- [92] J. Baur, N. Palanque-Delabrouille, C. Yeche, A. Boyarsky, O. Ruchayskiy, E. Armengaud, and J. Lesgourgues, Constraints from Ly- α forests on non-thermal dark matter including resonantly-produced sterile neutrinos, *J. Cosmol. Astropart. Phys.* **12** (2017) 013.
- [93] R. Murgia, V. Irsic, and M. Viel, Novel constraints on noncold, nonthermal dark matter from Lyman- α forest data, *Phys. Rev. D* **98**, 083540 (2018).
- [94] N. Palanque-DeLabrouille, C. Yèche, N. Schöneberg, J. Lesgourgues, M. Walther, S. Chabanier, and E. Armengaud, Hints, neutrino bounds and WDM constraints from SDSS DR14 Lyman- α and Planck full-survey data, *J. Cosmol. Astropart. Phys.* **04** (2020) 038.
- [95] W. Enzi *et al.*, Joint constraints on thermal relic dark matter from strong gravitational lensing, the Lyman- α forest, and Milky Way satellites, [arXiv:2010.13802](https://arxiv.org/abs/2010.13802).
- [96] A. Boyarsky, J. Lesgourgues, O. Ruchayskiy, and M. Viel, Lyman-alpha constraints on warm and on warm-plus-cold dark matter models, *J. Cosmol. Astropart. Phys.* **05** (2009) 012.
- [97] G. Ballesteros, M. A. G. Garcia, and M. Pierre, How warm are non-thermal relics? Lyman- α bounds on out-of-equilibrium dark matter, *J. Cosmol. Astropart. Phys.* **03** (2021) 101.
- [98] L. Amendola *et al.*, Cosmology and fundamental physics with the Euclid satellite, *Living Rev. Relativity* **21**, 2 (2018).
- [99] D. Alonso *et al.* (LSST Dark Energy Science Collaboration), The LSST Dark Energy Science Collaboration (DESC) science requirements document, [arXiv:1809.01669](https://arxiv.org/abs/1809.01669).
- [100] A. Aghamousa *et al.* (DESI Collaboration), The DESI experiment part I: Science, targeting, and survey design, [arXiv:1611.00036](https://arxiv.org/abs/1611.00036).
- [101] N. Aghanim *et al.* (Planck Collaboration), Planck 2018 results. VI. Cosmological parameters, *Astron. Astrophys.* **641**, A6 (2020); **652**, C4(E) (2021).